A&A, 687, A173 (2024)
https://doi.org/10.1051/0004-6361/202348858

Astronomy & Astrophysics

GRB 180128A: A second magnetar giant flare candidate from the Sculptor Galaxy

Aaron C. Trigg[1], Eric Burns[1], Oliver J. Roberts[2], Michela Negro[1], Dmitry S. Svinkin[3], Matthew G. Baring[4], Zorawar Wadiasingh[5,6,7], Nelson L. Christensen[8], Igor Andreoni[6,9,10,⋆], Michael S. Briggs[11], Niccolò Di Lalla[12], Dmitry D. Frederiks[3], Vladimir M. Lipunov[13], Nicola Omodei[12], Anna V. Ridnaia[3], Peter Veres[11], and Alexandra L. Lysenko[3]

[1] Department of Physics & Astronomy, Louisiana State University, Baton Rouge, LA 70803, USA
e-mail: atrigg2@lsu
[2] Science and Technology Institute, Universities Space and Research Association, 320 Sparkman Drive, Huntsville, AL 35805, USA
[3] Ioffe Institute, 26 Politekhnicheskaya, St. Petersburg 194021, Russia
[4] Department of Physics and Astronomy – MS 108, Rice University, 6100 Main Street, Houston, TX 77251-1892, USA
[5] Astrophysics Science Division, NASA/GSFC, Greenbelt, MD 20771, USA
[6] Department of Astronomy, University of Maryland, College Park, MD 20742, USA
[7] Center for Research and Exploration in Space Science and Technology, NASA/GSFC, Greenbelt, MD 20771, USA
[8] Université Côte d'Azur, Observatoire de la Côte d'Azur, CNRS, Artemis, 06304 Nice, France
[9] Joint Space-Science Institute, University of Maryland, College Park, MD 20742, USA
[10] Astrophysics Science Division, NASA Goddard Space Flight Center, Mail Code 661, Greenbelt, MD 20771, USA
[11] Department of Space Science, University of Alabama in Huntsville, Huntsville, AL 35899, USA
[12] Department of Physics and Kavli Institute for Particle Astrophysics and Cosmology, Stanford University, Stanford, CA 94305, USA
[13] Department of Physics, Lomonosov Moscow State University, Sternberg Astronomical Institute, 119991 13, Univeristetskij Prospekt, Moscow, Russia

Received 5 December 2023 / Accepted 12 May 2024

ABSTRACT

Magnetars are slowly rotating neutron stars that possess the strongest magnetic fields known in the cosmos (10^{14}–10^{15} G). They display a range of transient high-energy electromagnetic activity. The brightest and most energetic of these events are the gamma-ray bursts (GRBs) known as magnetar giant flares (MGFs), with isotropic energies $E_{\rm iso} \approx 10^{44}$–$10^{46}$ erg. Only seven MGF detections have been made to date: three unambiguous events occurred in our Galaxy and the Magellanic Clouds, and the other four MGF candidates are associated with nearby star-forming galaxies. As all seven identified MGFs are bright at Earth, additional weaker events likely remain unidentified in archival data. We conducted a search of the *Fermi* Gamma-ray Burst Monitor database for candidate extragalactic MGFs and, when possible, collected localization data from the Interplanetary Network (IPN) satellites. Our search yielded one convincing event, GRB 180128A. IPN localizes this burst within NGC 253, commonly known as the Sculptor Galaxy. The event is the second MGF in modern astronomy to be associated with this galaxy and the first time two bursts have been associated with a single galaxy outside our own. Here we detail the archival search criteria that uncovered this event and its spectral and temporal properties, which are consistent with expectations for a MGF. We also discuss the theoretical implications and finer burst structures resolved from various binning methods. Our analysis provides observational evidence of an eighth identified MGF.

Key words. stars: magnetars – stars: neutron – gamma-ray burst: individual: GRB180128A

1. Introduction

A magnetar is a type of neutron star (NS) characterized by an extremely strong magnetic field, $>10^{14}$ G (Usov 1984; Duncan & Thompson 1992; Paczynski 1992; Thompson & Duncan 1995, 1996; Kaspi et al. 2003). There are about 30 identified magnetars within our Galaxy (Olausen & Kaspi 2014), and they are associated with star-forming regions (Gaensler 2004). These objects display a wide variety of high-energy transient activity: from short (sub-second) gamma-ray bursts (GRBs) to burst forests with hundreds or thousands of bursts within tens of minutes, to magnetar giant flares (MGFs), the most energetic class of transient event involving magnetars (see, e.g., Kaspi & Beloborodov 2017, for a recent review).

Magnetar giant flares are characterized by an intense initial pulse ("spike") with typically a millisecond-long rise time, peak energy in the gamma-ray band (in the MeV range), and total isotropic-equivalent energy $E_{\rm iso} \gtrsim 10^{44}$ erg. In the three most proximate MGFs, observations show that a long, decaying tail with a duration of several hundred seconds follows this pulse, the intrinsic energy of which is on the order of a few times 10^{44} erg. The rotation of the NS periodically modulates this tail. Given the extremely high peak luminosities of the initial spikes, detection of these emissions is possible for magnetars located in galaxies of the Local Group up to a distance of ∼10 Mpc (Burns et al. 2021) by sensitive instruments such as the *Fermi* Gamma-ray

⋆ Neil Gehrels Fellow.

Burst Monitor (GBM). Furthermore, Burns et al. (2021) show that a fraction (∼2%) of MGFs from nearby galaxies masquerade as short GRBs. This fraction is consistent with the limits from previous studies (Palmer et al. 2005; Ofek 2007; Hurley 2011; Svinkin et al. 2015). In contrast, at extragalactic distances, the modulated tail, which is indicative of a MGF, is too faint to be observed with current instruments due to sensitivity limitations (Hurley et al. 2005). Given these current limitations, the best method for identifying extragalactic MGF candidates is by looking for events that display the distinct property of prompt gamma-ray emission and are spatially aligned with nearby star-forming galaxies.

The current sample of known MGFs counts seven events, three of which happened locally (in the Milky Way and the Large Magellanic Cloud; Mazets et al. 1979, 1999; Feroci et al. 1999; Hurley et al. 1999, 2005; Palmer et al. 2005; Frederiks et al. 2007) and, due to their exceptional brightness, saturated all observing instruments at that time. The remaining four events, GRB 051103, GRB 070201, GRB 070222, and GRB 200415A, were found to have spatial alignment in 2D with the nearby star-forming galaxies M81, M31, M83, and NGC 253 (also called the Sculptor Galaxy), respectively (Ofek et al. 2006, 2008; Frederiks et al. 2007; Mazets et al. 2008; Hurley et al. 2010; Svinkin et al. 2021; Roberts et al. 2021; Burns et al. 2021). After the completion of our current work, another extragalactic MGF candidate, GRB 231115A, was detected and localized to the galaxy M82 (Mereghetti et al. 2024; Wang et al. 2023; Yin et al. 2024; Minaev et al. 2024). Despite this small sample of events, Burns et al. (2021) reported a very high intrinsic volumetric rate of $R_{\rm MGF} = 3.8^{+4.0}_{-3.1} \times 10^5\,{\rm Gpc^{-3}\,yr^{-1}}$, supporting the idea that a commonly occurring progenitor, such as regular core-collapse supernovae, is at the origin of magnetars and that some must produce multiple MGFs, which would help inform our understanding of the mechanisms that cause them.

Section 2 relates our method for initially reducing the considered GRB sample and the procedures for further down-selecting MGF candidates and identifying and localizing these detections. A detailed analysis of *Fermi*/GBM data for the newly found event and a side-by-side comparison with the other MGF associated with NGC 253 (GRB 200415) as well as a likely NS merger (GRB 150101B) follows in Sect. 3.1. Section 3.2 covers the *Fermi* Large Area Telescope (LAT) data analysis. Sections 3.3–3.5 outline our search for detections of this event in other signals. In Sect. 4 we discuss the relativistic wind model for MGFs and how it relates to GRB 180128A, as well as the multi-pulse characteristics seen in the light curves of this new MGF candidate and three others, and the implications of finding a second burst localized to NGC 253. Finally, we conclude our findings in Sect. 5.

2. MGF identification

The *Fermi* GBM consists of 12 un-collimated thallium-doped sodium iodide (NaI) detectors and two bismuth germanate (BGO) detectors. The NaI and BGO detectors are arranged on opposite sides of *Fermi* (n0-n5 and b0 on one side and n6-nb and b1 on the other), with the NaI detectors oriented to observe the entire unocculted sky. The effective spectral ranges of the NaI and BGO detectors are ∼8–900 keV and ∼0.25–40 MeV, respectively, resulting in a combined spectral range of ∼8 keV to 40 MeV. To date, several catalogs detailing GRB data collected by the *Fermi* GBM (Gruber et al. 2014; Von Kienlin et al. 2014, 2020; Bhat et al. 2016) have been released. The events listed in these catalogs are generally longer and have longer variability timescales than MGFs (Gruber et al. 2014; Von Kienlin et al. 2014, 2020; Bhat et al. 2016). More information about the GBM instrument is available in Meegan et al. (2009).

Extragalactic candidate MGFs can be distinguished from regular short GRBs as the former show a shorter rise time and pulse duration, higher spectral energy peak, and are associated with host galaxies at distances appropriate to produce a given peak luminosity ($L_{\rm p} \sim 10^{41}-10^{47}\,{\rm erg\,s^{-1}}$) at Earth. We scoured the archival *Fermi*/GBM data, as we expected more MGFs (∼2–3) would be present. Following the success of past population searches, it has been confirmed that MGFs have the properties of sharp, millisecond-long rise times and extremely short peak interval durations. This allowed us to utilize these properties to first down-select the GRB sample considered before performing localization comparisons with nearby galaxies. A search of the entire short GRB population will identify MGFs at the expense of search sensitivity. Narrowing the considered sample provides enhanced statistical power over previous works by reduction of trials factors. Here, we describe the data and the methods used to discern MGF candidates from the pool of GBM triggers.

In this work we utilized the time-tagged event (TTE) data collected in the *Fermi*/GBM catalog until August of 2022. TTE data are generated for each detector with a 2 µs temporal resolution, with each photon tagged by the arrival time and one of the 128 energy channels, with separate channels for the NaI and BGO detectors. To analyze the data, we used the GBM Data Tools (Goldstein et al. 2022). We then applied a Bayesian blocks (BB) analysis (Scargle et al. 2013) to search for significant pulses in the light curves. Since the majority of extragalactic MGFs generally have durations of <100 ms (Burns et al. 2021, and references therein), our first event selection criterion was to select only the events in the catalog with a T_{50} smaller than 100 ms. The T_{50} is the duration over which 50% of the burst fluence accumulates. The start of the interval is when 25% of the total fluence is detected, measured between 50 keV and 300 keV. Applying the threshold to T_{50} instead of T_{90} (i.e., the duration during which 5%–95% of the burst fluence accumulates over the same energy range) should prevent the removal of any real, fainter MGFs. We then collected bcat detector mask[1] information to determine the best viewing subset of detectors for a given burst. This information indicates which NaI detectors contribute to "bcat" files, which provide basic information on a given burst, such as duration, peak flux, and fluence. We can select the appropriate BGO detector data based on which side (defined above) of *Fermi* has more NaI detectors used in the bcat files. This initial selection yielded a list of 137 possible MGF candidates.

Using the default parameters, we applied the BB algorithm in `astropy`[2] to the detector data and selected events for which the most significant BB bin is shorter than 20 ms. This value is short enough to discard any longer types of GRBs but still long enough to include the entirety of the initial prompt emission of previously identified MGFs. To ensure consideration of only events with very sharp rise times, we required that the first significant BB bin happen within 10 ms of the most significant BB bin. We defined significant bins as those with a signal-to-noise ratio greater than 3.5. The background is estimated for each burst using the BackgroundFitter module in GBM Data Tools. This module fits the background data using a second order polynomial over intervals before and after the burst, defined as from

[1] https://heasarc.gsfc.nasa.gov/w3browse/fermi/fermigbrst.html
[2] https://docs.astropy.org/en/stable/api/astropy.stats.bayesian_blocks.html

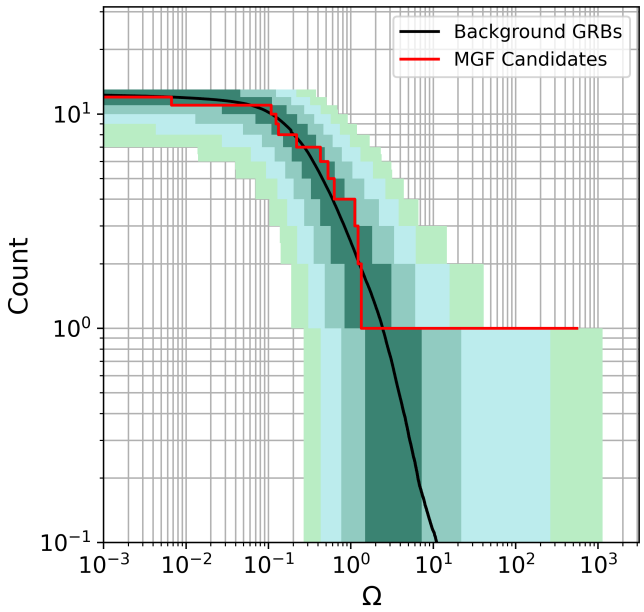

Fig. 1. Significance of the selected sample of 13 MGF candidates. Ω is a ranking statistic representing the believability that a given burst is a giant flare based on 3D spatial agreement with cataloged galaxies, as described in Burns et al. (2021). The red line indicates the 13 MGF candidates, and the black line represents the background distribution of GRBs. The green-shaded regions represent the 1, 2, 3, and 4σ two-sided confidence intervals. There is a single event outlier at 3.3σ significance: GRB 180128A.

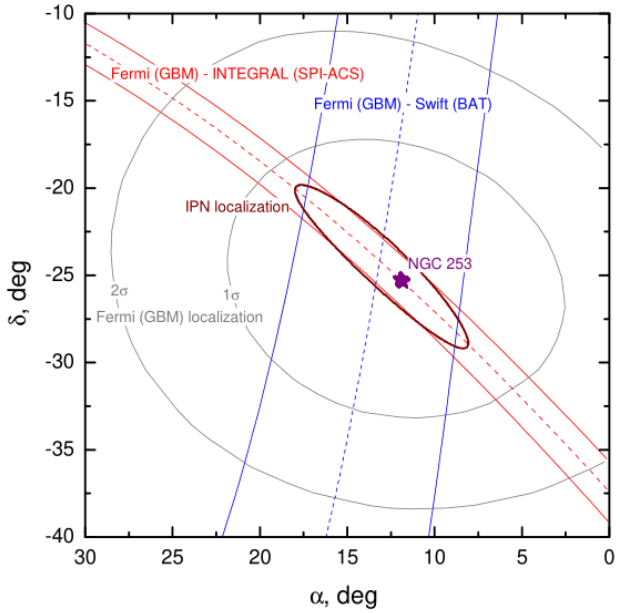

Fig. 2. Final IPN localization of GRB 180128A. The localization defined by the *Fermi*-INTEGRAL (red) and *Fermi-Swift* (blue) annuli. The shown annuli widths have 3σ confidence. The overlap of the annuli gives an ellipse (purple) with a 90% confidence area of 9.3 deg^2. The star marks the location of NGC 253. The initial *Fermi*/GBM localization and confidence intervals are in gray.

$T_0 - 15.1$ s to $T_{90\mathrm{start}} - 0.5$ s and from $T_{90\mathrm{stop}} + 1.0$ s to $T_0 + 15.1$ s. It then interpolates the background data to the time bins -15 s–15 s (Goldstein et al. 2022). After this step, 20 event candidates remained. We further removed events with known redshifts, as the isotropic luminosity for events at these distances would exclude a MGF origin. We also eliminated the MGF previously identified by Burns et al. (2021), leading to a considered sample of 13 MGF candidates.

The autonomous localization capability of *Fermi*/GBM is insufficient to robustly associate a GRB with a host galaxy. Thus, the Interplanetary Network (IPN) constructed annuli for these 13 events. Two of these events were detected only by *Fermi*/GBM. Five others have detections by *Fermi*/GBM and INTEGRAL (von Kienlin et al. 2003), which only constrained the annuli that reduce the GBM localization.

The remaining six events have detections by *Fermi*/GBM, INTEGRAL, and *Swift* Burst Alert Telescope (BAT; Barthelmy et al. 2005). We note that none of the MGF candidates have *Swift*/BAT localizations.

To quantify the significance of a given candidate to be a local MGF, we followed the procedure described in Burns et al. (2021) and Negro & Burns (2023). For each of the 13 GRBs in the sample, we constructed two spatial probability density functions (PDFs), represented in the HEALPix format. The first is P_i^{GRB}, which represents the localization probability of the GRB, where i is the pixel in the HEALPix map generated at an NSIDE = 8192 resolution. Distinct from this is P_i^{MGF}, which is a representation of the expected local spatial distribution for MGFs to have the given burst fluence at Earth. Each local galaxy, taken from Leroy et al. (2019) and Karachentsev et al. (2013), is weighted linearly by its star formation rate (SFR), equally distributed over its apparent size, and by the prevalence of MGFs, which is inferred from the E_{iso} from the given galaxy distance and GRB fluence pairing. All galaxies in the sample are placed on the sky to create P_i^{MGF}. That is, $P_i^{\mathrm{MGF}} \propto \mathrm{SFR}\times\mathrm{PDF}(E_{\mathrm{iso}}(d, S))$ where d is the host galaxy distance and S the fluence. Here the E_{iso} PDF is a power law that spans from 4.3×10^{44} erg to 5.8×10^{47} erg and utilizes the final measured value of $\alpha = 1.7 \pm 0.4$ (Burns et al. 2021). P_i^{MGF} is also normalized to unity.

These two distributions are combined to calculate the ranking statistic $\Omega = 4\pi \sum_i P_i^{\mathrm{GRB}} P_i^{\mathrm{MGF}} / A_i$, the product of the probabilities of the PDFs in the ith region of the sky of area A_i. This represents the believability that a given burst is a giant flare based on 3D spatial agreement with the cataloged galaxies (Fig. 1). The significance is determined by comparing the false alarm rate to a background distribution generated by random rotations of the sky (i.e., rotations of P_i^{MGF}) against the fixed P_i^{GRB}.

Among all the candidates, the GBM trigger bn180128215, hereafter GRB 180128A, was immediately identified as a strong candidate, standing out against the background distribution at 3.3σ significance. The remainder of this article focuses on the detailed analysis of this event; the population study will be the subject of future work.

Initially, the event was localized to an RA = 12.3 and Dec. = −26.1 degrees (J2000) by *Fermi*/GBM, with an average error ellipse radius of 5.7 degrees (Connaughton et al. 2015). Detection of GRB 180128A also exists for *Swift*/BAT (Barthelmy et al. 2005) outside of its coded field of view, and the anti-coincidence shield of the spectrometer aboard INTEGRAL (SPI-ACS; von Kienlin et al. 2003). The IPN refined the localization to 9.3 deg^2, which is centered on NGC 253, as shown in Fig. 2. In further investigating this event as having a MGF origin, we performed spectral and temporal analyses for this burst.

3. Prompt MGF analysis

For GRB 180128A, we analyze the *Fermi*/GBM data and search for signals in *Fermi*/LAT. We then compare the results with

Table 1. Time-resolved spectral analysis using BB.

Time (ms)	E_p (keV)	α	Energy flux ($\mathcal{F}$) ($\times 10^{-6}$ ergs s^{-1} cm^{-2})	L_{iso} ($\times 10^{47}$ erg· s^{-1})	E_{iso} ($\times 10^{45}$ erg)
GRB 180128A					
−12:−10	250 ± 50	6.0 ± 4.9	17.1 ± 4.6	0.28 ± 0.08	0.06 ± 0.02
−10:−7 (Peak 1)	560 ± 140	0.7 ± 0.6	64.5 ± 9.5	1.1 ± 0.2	0.32 ± 0.05
−7:−3	400 ± 120	8.2 ± 13.2	10.3 ± 4.1	0.17 ± 0.07	0.07 ± 0.03
−3:−1 (Peak 2)	490 ± 150	0.7 ± 0.8	50 ± 10	0.75 ± 0.17	0.15 ± 0.03
−1:18	190 ± 20	4.9 ± 2.3	3.7 ± 0.7	0.060 ± 0.010	0.12 ± 0.02
18:143	120 ± 30	1.6 ± 1.7	0.40 ± 0.11	0.007 ± 0.002	0.08 ± 0.02
T_{BB} duration (155):	290 ± 50	0.6 ± 0.5	2.4 ± 0.4	0.039 ± 0.007	0.60 ± 0.10
GRB 200415A					
−4.3:−3.9 (Peak 1)	320 ± 50	0.5 ± 0.4	170 ± 20	2.7 ± 0.4	0.11 ± 0.02
−3.9:−3.4	1100 ± 700	−0.8 ± 0.3	120 ± 60	2.0 ± 0.9	0.10 ± 0.05
−3.4:−2.9 (Peak 2)	800 ± 130	−0.1 ± 0.2	490 ± 80	8.0 ± 1.3	0.40 ± 0.07
−2.9:−2.5 (Peak 3)	1100 ± 200	−0.50 ± 0.14	850 ± 140	14 ± 2	0.56 ± 0.10
−2.5:−0.5 [†]	1210 ± 120	−0.1 ± 0.1	630 ± 60	10.5 ± 1.0	2.1 ± 0.2
−0.5:3.0	2040 ± 180	−0.16 ± 0.08	600 ± 50	10.0 ± 1.0	3.4 ± 0.3
3.0:5.0 [*]	900 ± 200	0.1 ± 0.3	110 ± 30	1.8 ± 0.4	0.36 ± 0.07
5.0:6.5 [*]	Completely in the data gap				
6.5:22.5 [*]	1040 ± 80	0.8 ± 0.2	124 ± 9	2.0 ± 0.2	3.3 ± 0.2
22.5:65.8	830 ± 50	0.46 ± 0.13	51 ± 3	0.84 ± 0.05	3.7 ± 0.2
65.8:93.4	590 ± 70	0.3 ± 0.2	19 ± 2	0.31 ± 0.03	0.85 ± 0.09
93.4:121.2	430 ± 50	0.8 ± 0.4	9.7 ± 1.1	0.16 ± 0.02	0.44 ± 0.05
121.2:150.3	250 ± 40	0.9 ± 0.6	3.1 ± 0.5	0.051 ± 0.007	0.15 ± 0.02
T_{BB} duration (155) [††]:	998 ± 40	0.04 ± 0.05	56 ± 2	0.91 ± 0.04	14.2 ± 0.5
GRB 150101B					
−16:−8 (Peak 1)	1100 ± 600	−0.4 ± 0.4	16 ± 7	8000 ± 4000	6000 ± 3000
−8:−2 (Peak 1)	220 ± 70	−0.8 ± 0.3	6.3 ± 1.3	3200 ± 700	1900 ± 400
−2:4	61 ± 12	0.3 ± 1.2	1.4 ± 0.3	730 ± 150	440 ± 90
4:74	25 ± 6	−0.8 ± 1.0	0.35 ± 0.05	180 ± 30	1300 ± 200
T_{BB} duration (90):	150 ± 80	−1.5 ± 0.2	1.1 ± 0.2	550 ± 120	4100 ± 900

Notes. The fluence is from fitting the spectrum with a Comptonized function over a combined (NaI and BGO detectors) spectral range of 8 keV–40 MeV. [†]Includes the saturated portion of the spectrum from about $T_0 - 2.4$ to −0.8 ms. [*]Includes the data gap, from about $T_0 + 4.6$ to 6.6 ms. [††]This does not include the correction for the brightest part of the event that was saturated in *Fermi*/GBM as in Roberts et al. (2021), which accounts for the lower values in this study.

those from two other GRB detections with a confident progenitor classification, allowing us to compare the characteristics of GRB 180128A with those of a known MGF and a GRB produced by another source.

3.1. Fermi/GBM analysis of GRB 180128A

GRB 180128A triggered GBM on January 28, 2018, at 05:09:56.60 UT. We generate responses for detectors viewing that position within 60° of their boresight. The initial T_{50} and T_{90} durations of GRB 180128A were found to be 48 ± 51 ms and 208 ± 400 ms, respectively (Von Kienlin et al. 2020). These error bars are typical for short-duration bursts where the total fluence is almost comparable to background fluctuations in GBM. Reanalyzing this event using BB analytical techniques (Scargle et al. 2013), we find a duration (T_{BB}) of 155 ms. This duration include a 125 ms tail with a signal-to-noise ratio of 6.5. Without this moderate significance tail the dominant emission interval is 30 ms long.

We initially fit the differential energy spectrum of GRB 180128A with models typically employed for GRBs (Von Kienlin et al. 2020) and for MGFs (Roberts et al. 2021; Svinkin et al. 2021; Kaspi & Beloborodov 2017). These fits included a simple power-law model and a Band function (Band et al. 1993). In addition, our spectral fitting models focused on a Comptonized function (COMPT; Gruber et al. 2014), a form common to magnetar burst studies (e.g., Lin et al. 2011). The function is a power law of index α modulated by an exponential cutoff at a characteristic energy E_p that is close to the spectral peak in a νF_ν representation. The values of α and E_p for GRB 180128A, and the two comparison bursts are listed in Table 1 for an array of BB time bins, defining the spectral evolution of these transients. To better illustrate the soft-to-hard-to-soft evolution that is the envelope behavior of this burst, we plotted four of the BB intervals of GRB 180128A. The results in Fig. 3 exhibit the spectral evolution from the onset of the burst to the two peaks to the extended emission after the peaks. For clarity, we omitted the third and fifth BB intervals from Fig. 3. They are, however, consistent with the trend seen in the displayed intervals. Notably, this spectral evolution is reminiscent of that clearly evident in the MGF GRB 200415A.

We performed a time-integrated fit using a COMPT model to the *Fermi*/GBM data for GRB 180128A over energies 8 keV–40 MeV, and the beginning and end of the significant emission as defined by the BB analysis, the results of which are in Table 1. We note that a Band model fits the spectrum equally

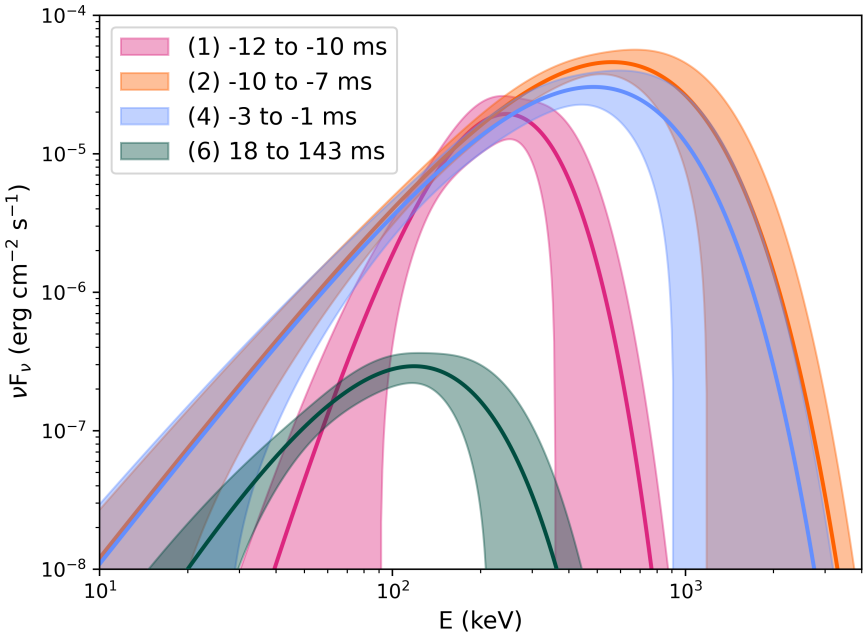

Fig. 3. Spectra of GRB 180128A over four BB time intervals. The intervals show the onset of the burst (1), peak 1 (2), peak 2 (4), and the extended emission after the peaks (6). Intervals (3) and (5) are omitted for clarity but are consistent with the trend displayed. The shaded area indicates the 1σ confidence regions.

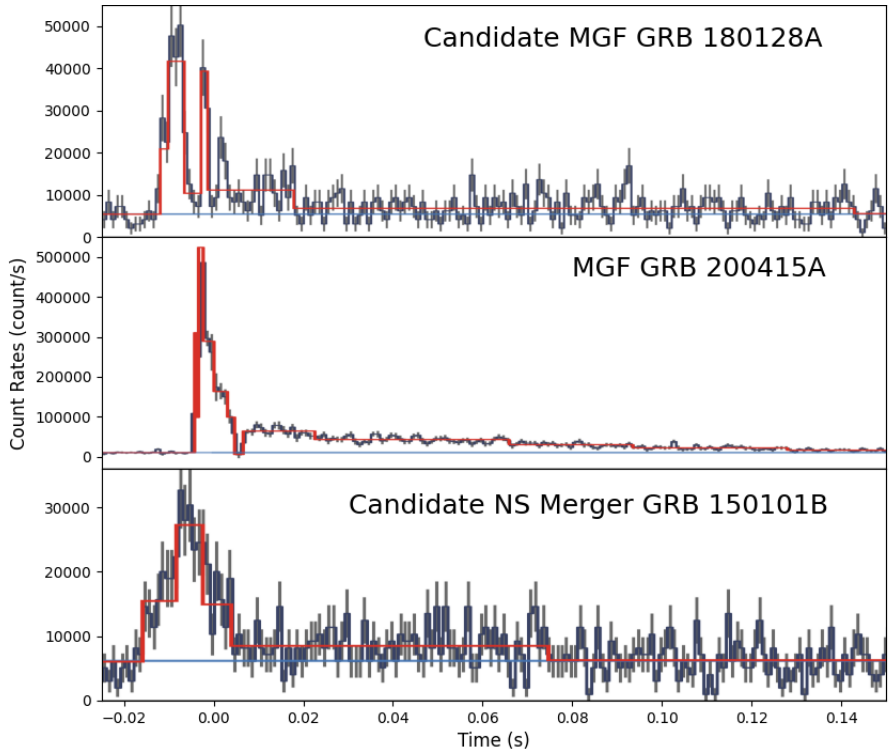

Fig. 4. Light curves of the events GRB 180128A, GRB 200415A, and GRB 150101B, binned to a temporal resolution of 1 ms for energies from 10–500 keV. The black lines represent the raw data. The gray line shows the energy-integrated background. The red lines show the significance of the pulses above the background (gray line) using a BB algorithm. At this temporal resolution, GRB 180128A displays two distinct millisecond peaks.

well but with more poorly constrained values. Using the distance to NGC 253 of 3.7 Mpc (at this distance, we neglected cosmological redshift; Leroy et al. 2019), we find an $E_{\rm iso} = (5.9 \pm 1.0) \times 10^{44}$ erg from the fluence values of the COMPT fit to the spectrum over the BB duration of 155 s. We also find an $L_{\rm iso} = (3.9 \pm 0.7) \times 10^{45}$ erg s^{-1} from the fluence and flux values for the same model fit and duration.

We first compared the spectroscopy of our burst with that for the MGF GRB 200415A (Svinkin et al. 2021; Roberts et al. 2021), the only other MGF clearly identified by *Fermi*/GBM up to now, fitting the BB time bins shown in red for the light curves in Fig. 4. The $L_{\rm iso}$ and $E_{\rm iso}$ determinations for GRB 180128A and GRB 200415A were consistent with those expected from a MGF and are given in Table 1 for each BB time interval, along with those for GRB 150101B. For GRB 200415A and GRB 150101B, the values from our time-integrated COMPT model analysis (also listed in Table 1) were consistent with those obtained in Roberts et al. (2021) and Burns et al. (2018), respectively. It is worth noting that the $E_{\rm iso}$, $E_{\rm p}$, and α values list for GRB 180128A and GRB 200415A fall within the values of all other known MGFs (Burns et al. 2021): with α ranging from around 0.0 to 1.0 and $E_{\rm p}$ starting around 300 keV and extending as high as several MeV.

Table 2. *Fermi*/LAT results.

Name	Flux ($cm^{-2}\ s^{-1}$)	Energy flux ($erg\ cm^{-2}\ s^{-1}$)	L_{iso} ($erg\ s^{-1}$)	E_{iso} (erg)
GRB 180128A	$<1.9 \times 10^{-6}$	$<2.3 \times 10^{-10}$	$<3.7 \times 10^{41}$	$<1.8 \times 10^{44}$
GRB 200415A	$(4.1 \pm 2.2) \times 10^{-6}$	$(4.8 \pm 2.7) \times 10^{-9}$	$(7.4 \pm 4.2) \times 10^{42}$	$(3.6 \pm 2.1) \times 10^{45}$
GRB 150101B	$<4.9 \times 10^{-6}$	$<1.9 \times 10^{-9}$	$<9.4 \times 10^{46}$	$<2.8 \times 10^{50}$

Notes. Comparison between the LAT detection of GRB 200415A and the upper limit on GRB 180128A and GRB 150101B. For the latter, we assumed $z = 0.134$ for the associated host galaxy ($D = 0.65$ Gpc) Fong et al. (2016), and we used the same analysis setup as for GRB 180128A (see the main text). All fluxes and energy fluxes measured from 0.1 to 10 GeV.

The detection of GRB 150101B by *Swift*/BAT localized its position well (Cummings 2015), so that follow-up observations determined a host galaxy redshift $z = 0.134$ (Fong et al. 2016), corresponding to a source distance of 0.65 Gpc from Earth using the most recent Planck Collaboration Λ cold dark matter cosmology parameters (Planck Collaboration VI 2020). This distance is over two orders of magnitude greater than that of NGC 253, implying that this event is several orders of magnitude more luminous than the known Galactic MGFs. We chose GRB 150101B for comparison because it is one of the seven candidates that met all of our initial temporal selection criteria, but the known distance excludes a MGF origin. This transient is likely the result of a NS merger, analogous to GRB 170817A (Goldstein et al. 2017; Troja et al. 2018; Burns et al. 2018).

The light curve of GRB 150101B consists of a 16 ms spike followed by a longer, softer decaying tail that lasts around 64 ms, for a total event duration of around 80 ms (Burns et al. 2018), and is generated using the same criterion for determining detectors with good angles relative to the source (i.e., angle <60° to boresight). Given the cosmological distance, we cannot neglect cosmological redshift. Therefore, to calculate the L_{iso} and E_{iso} of the time-resolved and time-integrated spectra, we must k-correct the energy measurements (Bloom et al. 2001).

3.2. Fermi/LAT analysis of GRB 180128A

The *Fermi*/LAT (Atwood et al. 2009) detected high-energy emission from the NGC 253 MGF in April 2020 (GRB 200415A; Ajello et al. 2021). The detection consisted of three photons between 0.48 and 1.7 GeV. The arrival time of the first photon was delayed with respect to the GBM trigger by ~19 s, with the last photon detected ~284 s later. With the tight sky localization of these photons compatible with the location of NGC 253 and the approximate temporal coincidence with the MGF, these data represented the first ever *Fermi*/LAT detection in the GeV energy band of emission from a magnetar.

For GRB 180128A, NGC 253 was well within the LAT field of view at the moment of the trigger and remained visible until ~3000 s after. We find no significant detection at the source location and place an upper limit on the source flux. We performed a likelihood analysis with `gtburst`[3], using P8R3 data with TRANSIENT10e source class, and select events within a 5-degree radius from the target, with energy between 100 MeV and 10 GeV in a time window between 0 and 3000 s from the trigger time. Assuming a power-law spectrum with an index $\Gamma = -2.1$, we find an energy flux upper limit of 2.3×10^{-10} erg cm^{-2} s^{-1}. Considering an integration time of 3000 s and the distance to NGC 253 of 3.7 Mpc, the limit on the intrinsic total energy above the LAT threshold is $E_{iso} < 1.8 \times 10^{44}$ erg at a 95% confidence level. The LAT detection of GRB 200415A had an estimated intrinsic energy of $(3.6 \pm 2.1) \times 10^{45}$ erg in the 0.1–10 GeV band, almost one order of magnitude higher than the upper limit we find in this work. The non-detection of GRB 180128A clearly rules out any notion that all MGFs have a GeV counterpart of similar strength.

Yet, we cannot a priori exclude that the GeV emission observed by LAT scales quasi-linearly with the soft gamma-ray luminosity detected by the GBM. To assess this possibility and consistently compare GRB 180128A with GRB 200415A, we repeated the analysis routine with the same setup as in Ajello et al. (2021), namely with `P8_TRANSIENT020E` events in a time window 10–500 s from the GBM trigger. This time, we selected a region of 12 degrees radius to match the analysis setup of GRB 200415A chosen to accumulate enough background statistics to allow a better fit of the Galactic diffuse and isotropic emissions. According to this setup, the upper limit at 95% C.L. on the intrinsic luminosity in the 0.1–10 GeV energy range is $L_{iso} < 2.3 \times 10^{42}$ erg/s ($E_{iso} < 1.1 \times 10^{45}$ erg), more than a factor of 11 above the predicted value given by the simple scaling of the intrinsic energetic luminosity found for GRB 200415A. The upper limits we obtained using this setup are significantly larger, by an order of magnitude, compared to the limits for GRB 180128A obtained with the previous setup and listed in Table 2. These new limits are much closer to the values listed in Table 2 for GRB 200415A.

3.3. Optical

To rule out the possibility that GRB 180128A was due to other transient candidates visible in the optical band, we conducted searches of the data from the *Zwicky* Transient Facility (ZTF; Graham et al. 2019; Bellm et al. 2019) and MASTER (Lipunov et al. 2010, 2022). ZTF data show no obvious candidates, ruling out a supernova and the typical afterglow at the distance of NGC 253. However, there are no observations between December 12, 2017, and July 22, 2018, the range that overlaps the trigger time of our event. The MASTER observations covered ~3/4 of the IPN localization up to February 4 (~8 days after the burst) with no optical transient detections down to ~17–19 mag, which suggests that the burst was likely not associated with a supernova.

3.4. Gravitational waves

The Laser Interferometer Gravitational-Wave Observatory (LIGO; LIGO Scientific Collaboration 2015) and Virgo (Acernese et al. 2014) were offline at the time of the

[3] https://fermi.gsfc.nasa.gov/ssc/data/analysis/scitools/gtburst.html

event, having ended the second observing run on August 25, 2017[4]. Hence, there are no gravitational wave (GW) data to determine whether this event might be due to a NS merger.

LIGO and Virgo also have searches targeting GWs produced from magnetars (Abadie et al. 2011; Abbott et al. 2021), including those associated with MGFs (Abbott et al. 2019; Macquet et al. 2021). Even in the absence of direct detection, it is possible to set upper limits on the GW energy emission. In fact, during the Galactic MGF of December 27, 2004 (Palmer et al. 2005), LIGO reported an upper limit on the energy emission (Abbott et al. 2007). However, since this initial reporting, the sensitivity of LIGO detectors has increased ∼100x. Given this increase in sensitivity, the LIGO-Virgo-KAGRA observations from future observing runs (Abbott et al. 2020) will provide important information for describing the energetics of identified MGFs.

3.5. Radio

Associations between fast radio bursts (FRBs) and coincident X-ray bursts from magnetars (Bochenek et al. 2020) have led to the development of models for these phenomena consistent with MGFs. Despite NGC 253 being "radio-loud" due to a prominent synchrotron radio halo (Carilli et al. 1992), to determine if there were any FRBs detected coincident with GRB 180128A, we consulted the FRB[5] (Petroff et al. 2016) and CHIME[6] (CHIME/FRB Collaboration 2021) catalogs. The FRB catalog lists two unverified events on the same day as GRB 180128A. However, both detection localizations are far outside the IPN localization for our event. No relevant events listed in the CHIME catalog coincide with the time or location of GRB 180128A. A search of the Very Large Array archive (Perley et al. 2011) also found no observations around the time of our event.

4. Discussion

Many of the characteristics seen in GRB 180128A can be explained by current MGF theory. However, it displays several properties that make it an interesting event. The first is the appearance of two distinct peaks in the light curve. The other interesting point is that this burst was localized to the same galaxy as another known MGF, making it the first time multiple MGFs are associated with the same galaxy outside the local neighborhood. Also of interest is how different binning techniques affect how the relativistic wind structures are resolved. Here, we discuss the implications of these properties.

4.1. Physical mechanisms and spectral-flux correlations in Fermi/GBM data for the giant flare candidates

The energetics analysis in Sect. 3 can be interpreted as a result of a large-scale crustal disruption event (Norris et al. 1991; Thompson & Duncan 1995). Due to a build-up of magnetic stresses in the crust, the stellar crust reaches a breaking point and can shear and crack, rapidly heating the local plasma. This powerful event launches a hot, relativistic pair–photon fireball with little baryonic contamination into the magnetosphere (Thompson & Duncan 1995), accompanied by magnetic reconnection as the plasmoid is ejected. The fast initial pulse of GRB 180128A is consistent with this very large release of magnetic energy (Thompson & Duncan 1995, 1996).

The classification of GRB 180128A as a MGF came from the initial selection criteria and localization. The analysis shows it is consistent with a MGF origin. Furthermore, insights into the MGF physical emission region and mechanism originate from considerations of the spectral evolution and the coupling between spectral and flux variations. We focused on the νF_ν peak energy E_p. For the bright GRB 200415A, the values for the power-law index, α, in the COMPT spectral fits are generally in the range 0−1 (see Table 1). This is commensurate with expectations from polar winds in MGFs due to the high opacity of Compton scattering by electrons in the strong magnetic fields (Roberts et al. 2021). For our spectral-flux correlation analysis of GRB 200415A, we employed the α values determined from the COMPT fit, which match those of Roberts et al. (2021) for Figs. 5 and 6a. In contrast, because the count statistics for GRB 180128A and GRB 150101B was poorer, and in some cases unconstrained, we fixed the power-law index to $\alpha = 1.0$ and $\alpha = 0.0$, respectively, for Figs. 5 and 6a (Table A.1). These values assume both bursts have a MGF origin: GRB 180128A having a lower energy, we expected an α closer to 1.0, while GRB 150101B has a much higher energy, which would lead to an expected α value closer to 0.0. Any deviation from behaviors expected from a MGF using these values would strongly disfavor a likely MGF origin. For all three bursts in Fig. 6b, the adopted α values are those listed for the BB interval choice in Table 1.

Figure 5 plots the evolution of E_p values for our two selected MGF candidates plus GRB 150101B, with data for each burst acquired using 8 ms temporal binning (Table A.1). It displays a quasi-exponential decay for GRB 200415A on a relatively long timescale (see also Roberts et al. 2021). GRB 180128A has a more rapid decay that is quasi-exponential at its outset. In contrast, GRB 150101B exhibits E_p values with a faster decay that quickly morphs into an E_p fluctuation.

Figure 6a presents the relationship between L_{iso} and E_p, also temporally binned to 8 ms intervals. For GRB 1801128A and GRB 200415A, we see a well-defined $L_{iso} \propto E_p^2$ relationship, which is a strong indicator of relativistic Doppler boosting (Roberts et al. 2021, see also just below). The $L_{iso} \propto E_p^2$ relation is not as readily recovered for GRB 150101B, which has fewer data points. Interestingly, when plotting the L_{iso}-E_p correlation using the BB intervals (omitting any data gaps or saturated data points) as in Fig. 6b, the fit index is no longer 2 (i.e., L_{iso} is not $\propto E_p^2$), and differs between the MGF candidates. The fit index for GRB 180128A is greater than 3, yet there is significant dispersion in the data points that closely matches the scatter in the time-dependent analysis of Chand et al. (2021). Moreover, we observe that the $L_{iso} \propto E_p^2$ relation can be recovered when fitting the lower L_{iso} intervals that correspond to the dips in the light curve of GRB 200415A. The four points above the fit line for GRB 200415A displayed in Fig. 6b correspond to the first four BB intervals (and thus the peaks in the light curve) in Table 1. This selective sampling suggests that the BB binning choice resolves the finer structures within the burst.

The dependence of the L_{iso}-E_p correlation on the temporal binning protocol is not unexpected, and it provides interesting insight into the observational sampling of a MGF wind. Roberts et al. (2021) interpreted the $L_{iso} \propto E_p^2$ coupling for GRB 200415A as being the signature of a relativistic wind emanating from the magnetar pole and collimated by the field lines (essentially a flared jet) that sweeps across an observer's line of sight as the star rotates. During this sweep, the effective Doppler factor δ_w sampled by *Fermi* GBM rises and falls, generating

[4] https://www.ligo.caltech.edu/page/timeline
[5] https://www.frbcat.org/
[6] https://www.chime-frb.ca/catalog

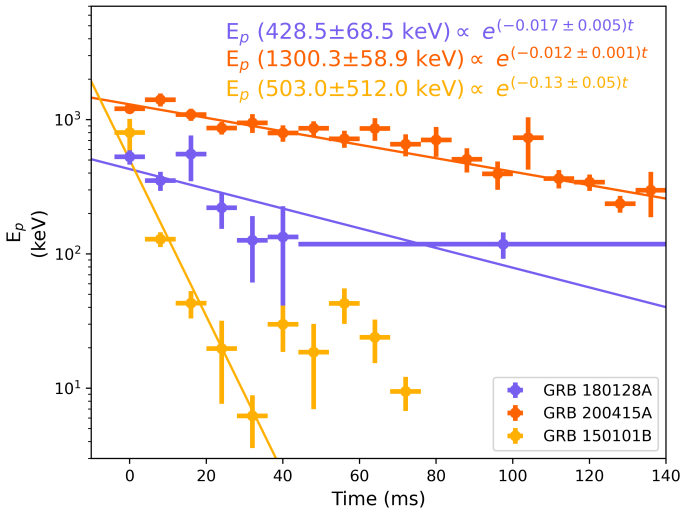

Fig. 5. Comptonized spectrum peak energy (E_p) as a function of time using a temporal binning of 8 ms and values from Table A.1. All fit errors and error bars are at the 1σ confidence level. The zero-time reflects the GBM event start time of each detection.

a spread in E_p, with $E_p \propto \delta_w$ for the photon energy Doppler blueshift, and a range in L_{iso}. For the temporally agnostic choice of fixed, 8 ms time bins, the cumulative flux in a bin tends to sample a broader range of wind axis orientations during the stellar rotation. From the perspective of the jet axis, this essentially integrates over a large solid angle $\Delta\Omega$ of the Doppler beam. Accordingly, the accumulated signal is a flux rather than an intensity and depends quadratically on the Doppler factor (i.e., $L_{iso} \propto \delta_w^2$) due to the combination of photon Doppler blueshift and time dilation in the Lorentz boost from the wind frame to that of the observer. Thus, the $L_{iso} \propto E_p^2$ relationship naturally emerges, as highlighted in the analysis of Roberts et al. (2021) and Fig. 6a for GRB 200415A, and also for GRB 1801128A.

In contrast, the BB approach inherently bins on shorter timescales for higher fluxes (see Fig. 4), corresponding to a narrower sampling of solid angles relative to the jet axis as the magnetar rotates. Then the detected signal scales more like intensity (i.e., the flux per unit solid angle), and this has the well-known Doppler boosting dependence $L_{iso} \propto \delta_w^4$ since $\Delta\Omega \propto \delta_w^{-2}$ defines the Doppler cone. Accordingly, one would then anticipate a $L_{iso} \propto E_p^4$ in this particular extreme. It is then no surprise that the BB display in Fig. 6b for GRB 200415A and GRB 180128A generates a stronger L_{iso}-E_p correlation than that observed for fixed time bins in Fig. 6a. The fit index being below four suggests that there is a partial sampling of the wings of the Doppler beam in the shortest BB time bins, which, in principle, possibly allows for an estimate of the ratio of the unknown rotation period to the bulk Lorentz factor $\Gamma \sim \delta_w$ of the MGF wind. Observe that the flat L_{iso}-E_p correlation for GRB 150101B cannot be explained by this picture. Its poorer count statistics and anomalous light curve suggest that other conditions prevail: its wind may not be ultra-relativistic, thereby limiting its Doppler beaming, with both being consistent with GRB 150101B resulting from a NS merger as opposed to being a MGF.

To determine the speed of the MGF winds, we employed a traditional GRB method: assessing the transparency of the highest energy photon (E_{max}) to pair creation ($\gamma\gamma \rightarrow e^+e^-$) to constrain the bulk Lorentz factor Γ. All emitted photons must escape the region, aided by relativistic Doppler beaming, which increases the effective pair threshold energy (Krolik & Pier 1991; Baring 1993). The most conservative bound, $\Gamma > E_{max}/511$ keV, arises from Doppler boosting of the 511 keV pair threshold from the wind's rest frame. For the GRB 200415A MGF, Roberts et al. (2021) reported $E_{max} \sim 3$ MeV in the GBM data (about a factor of 3 higher than the typical E_p listed in Table 1) and deduced $\Gamma \gtrsim 6$, though this is well below that inferred from the *Fermi*/LAT observations of delayed GeV photons (Ajello et al. 2021, see also just below). Using the Bayesian method described in Roberts et al. (2021) for the on-source/off-source signal detection (Fig. 7), the highest energy of photons from GRB 1801128A identified as being statistically significant above background is ~500 keV. Thus, pair transparency bounds on Γ are poorly defined for GRB 180128A and therefore uninformative.

4.2. Multi-pulse variability

It has historically been believed that MGFs have only single pulses, based on observations of the Galactic events GRB 790305B, GRB 980827, and GRB 041227. However, this belief was informed predominantly by saturated observations that would hide any multi-pulse structure within that part of the prompt burst emission. Therefore, studying extragalactic MGFs, which do not suffer from saturation effects, provides the opportunity to understand if MGFs can have multi-pulse temporal structure similar to those seen in short, lower-energy soft gamma repeater (SGR) bursts. The light curve of GRB 180128A displays two distinct pulses at sub-millisecond resolution (Fig. 4). This MGF candidate is the fourth event to display such behavior, the other three being GRB 070201 (Mazets et al. 2008; Ofek et al. 2008), GRB 070222 (Burns et al. 2021), and GRB 200415A (Roberts et al. 2021). In the case of GRB 070201, the temporal variability was used to argue against it having a MGF origin and raised the possibility that it was a background short GRB (Ofek et al. 2008), as such variability is consistent with short GRBs (Nakar & Piran 2002). These four account for roughly half of all likely events, the majority of which do not have sub-millisecond data, which may point to this being a common characteristic of MGFs, contrary to prior expectations.

The multi-pulse variability may imply repeated injections or varying observer geometry with the outflow. From Fig. 6a, it is apparent that GRB 180128A's inter-pulse traces $d\log L_{iso}/(d\log E_p) \sim 2$ as for other MGF candidates (and is distinct from GRB 150101B). This relation is compatible with the observer sampling varying Doppler factors when the outflow becomes optically thin. The multiple pulses then might be due to a similar origin from distinct persisting outflows; for example, the observer samples a hollow conal geometry of a narrow structured jet as it sweeps past. Alternatively, these multi-pulses may be due to actual variability of energy injections from the magnetar crust and magnetosphere into the outflow. These timescales are compatible with characteristic oscillation mode periods of the magnetar, ranging from ~50−100 ms for the lowest-order crustal torsional modes to milliseconds for f-modes. The latter is potentially important for GW searches of MGFs (Macquet et al. 2021).

4.3. Repeating magnetar probability calculation

GRB 180128A occurred only 808 days before GRB 200415A. The median volumetric rate of 3.8×10^5 Gpc^{-3} yr^{-1} (Burns et al. 2021) corresponds to 0.05 MGFs per 1.0 $M_\odot$ yr^{-1}. Given the star formation of NGC 253 (Leroy et al. 2019) a predicted rate of

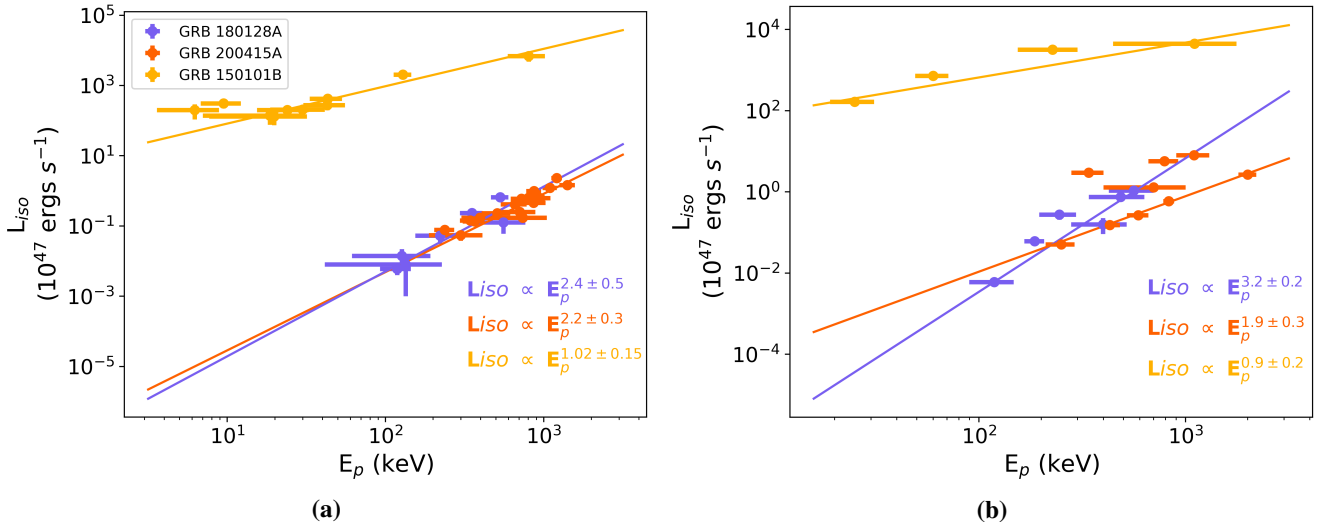

Fig. 6. Flux and spectral evolution of GRB 180128A (lavender), GRB 200415A (orange), and GRB 150101B (amber). *Left (a):* correlation between $L_{\rm iso}$ and $E_{\rm p}$ for all three transients, revealing an approximate $L_{\rm iso} \propto E_{\rm p}^2$ relationship that is a strong signature of relativistic winds. The temporal binning for panel (a) is uniformly 8 ms and uses the values in Table A.1. *Right (b):* $L_{\rm iso}$ and $E_{\rm p}$ for all three transients over the BB intervals in Table 1, omitting the data gaps and saturated intervals of GRB 200415A. All fit errors and error bars are at the 1σ confidence level.

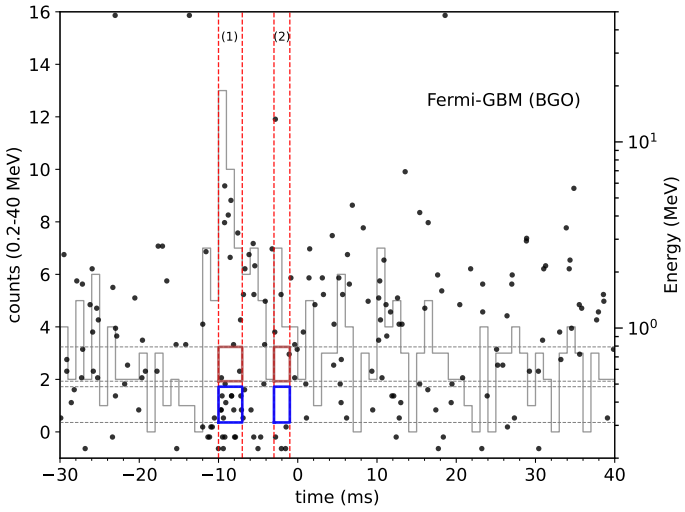

Fig. 7. Individual TTE data of GBM BGO detector 1 (black dots) for GRB 180128A. The blue rectangles indicate energies from 312 to 484 keV in intervals (1) and (2), corresponding to peaks 1 and 2. The red rectangles represent energies from 518 to 792 keV for the same time intervals. We conclude that the highest photon energy associated with GRB 180128A is ~500 keV.

0.24 MGFs $\rm yr^{-1}$ can be assumed. With an approximate assumption that the detection capability to MGFs of *Fermi*/GBM, INTEGRAL SPI-ACS, and *Swift*/BAT is half that of the broader IPN (ie. $\sim 6.0E{-}7\,\rm erg\,cm^{-2}$) we expect about 0.049 MGFs per year to be detectable by these satellites and thus identifiable as arising from NGC 253. With this rate, the Poisson probability (i.e., assuming uncorrelated events) of two within 808 days is ~10%. Improved estimates can better determine the sensitivity of these instruments and the loss of coverage by one or more due to live-time and occultation issues, but are unlikely to exceed 5%. Rejection of this assumption would suggest that a single, young magnetar is the source of MGFs well above the age-averaged MGF production rate for individual magnetars.

Nominally, this chance probability could be refined by accounting for the exposure and sensitivity in the observing instruments and the localization of GRB 200415A containing only a portion of NGC 253. Unfortunately, order of magnitude uncertainties currently dominate the intrinsic rate of MGFs. An unambiguous answer may be possible with more precise localizations of short GRBs. Below we detail the implications assuming the two events originate from a single magnetar.

Lower energy magnetar short bursts are highly correlated in time (i.e., non-Poisson). No observations exist of two MGFs from the same magnetar in our Galaxy. A time interval of 808 days is short, yet does not definitively indicate that the two MGFs emanate from the same magnetar, as ~2190 days separated the SGR 1900 and SGR 1806 MGFs that came from different NSs. The magnetar crust is thought to be in a self-organized critical state (e.g., Göğüş et al. 1999; Lander 2023); short bursts have a power-law event size distribution $\rm d\log N/d\log E_{iso} \sim -1.7$ (Cheng et al. 1996) and have temporal correlations in activity rate similar to earthquakes and associated aftershocks (Bak et al. 2002). It is unclear if the trigger for MGFs is entirely different from that for short bursts or if they are identical and MGFs are merely much rarer and larger events. A tentative calculation in Burns et al. (2021) suggests the short burst and MGF cumulative energy power laws are compatible and could smoothly connect over 10 orders of magnitude (within large uncertainties), favoring the scenario where the short burst and MGF physical triggering mechanism are fundamentally the same. This explanation could favor a more mature magnetar where the crust has had time to solidify and form strong stresses a few decades after formation (Lander 2023) from presumably a supernova.

If it is, in fact, the same magnetar, it would inform our understanding of the mechanism of MGFs and how stresses build and relax in the magnetar crust. Generally, magnetars in our Galaxy that have produced MGFs relax to less active states in the months or years following the event. The giant flares are energetic enough to putatively melt large zones of the outer crust, relieving stresses and large magnetic field twists. A second MGF would suggest a deep inner crust origin of the subsequent MGF trigger, matching expectations from some models (e.g.,

Lander et al. 2015; Kojima 2022). Statistics afforded by larger MGF populations are required to make definitive conclusions. Future proof of this would greatly benefit from the improved determination of the intrinsic rate uncertainties, as would newer high-energy wide-field monitors with arcminute-scale localizations.

5. Conclusions

Using the distinct MGF characteristic of prompt millisecond emission, paired with IPN localization to nearby star-forming galaxies, we have developed a robust and reproducible method for searching archival data for extragalactic MGFs weaker than those previously identified. In our initial results, GRB 180128A stands out as a strong candidate MGF, supporting expectations that weak MGFs remain unidentified in archival data. Continued searches of archival *Fermi*/GBM data and the data of other missions may reveal yet more hidden MGFs. GRB 180128A was subsequently localized to NGC 253, making it the fifth likely MGF candidate localized to a nearby galaxy and the second such event localized to that specific galaxy. This localization marks the first time multiple MGFs have been found in a galaxy outside our own, and future studies should be carried out to determine whether individual magnetars produce multiple MGFs. We have shown that the multi-pulse variability displayed in the light curves of GRB 180128A and other MGFs is a common trait. In our analysis of *Fermi*/LAT data for GRB 180128A, we did not detect the presence of GeV photons, contrary to the case of the MGF GRB 200415A, which indicates that not all MGFs produce GeV photons.

Through our analysis and comparison of GRB 180128A and GRB 200415A, we have advanced our understanding of the physical mechanisms of these events. We extended the relativistic wind model put forth in Roberts et al. (2021) for GRB 200415A and, using selective binning techniques, resolved the finer structures within GRB 180128A by changing the observational sampling of a MGF wind. Continued population studies will help determine whether this model can reveal variation within the source class and whether such relativistic wind scenarios for MGFs are universal.

Improving the rapid down-selection criterion for short GRBs enhances the algorithm's applicability in real-time systems, facilitating the rapid identification of potential MGFs for subsequent observations. These observations will aid in verifying the nature of these candidates as MGFs as they will allow us to investigate whether they are cosmological short GRBs originating from significantly distant hosts. Moreover, rapid follow-up observations that utilize both current and forthcoming X-ray missions may capture the long periodically modulated tail that is characteristic of an MGF.

Acknowledgements. AT, EB, MN, and OJR acknowledge NASA support under award 80NSSC21K2038. MN and ZW acknowledge the support by NASA under award number 80GSFC21M0002. MGB thanks NASA for generous support under awards 80NSSC22K0777 and 80NSSC22K1576. OJR gratefully acknowledges NASA funding through contract 80MSFC17M0022. The *Fermi*/LAT Collaboration acknowledges generous ongoing support from several agencies and institutes that have supported both the development and operation of the LAT and scientific data analysis. These include the National Aeronautics and Space Administration and the Department of Energy in the United States, the Commissariat à l'Energie Atomique and the Centre National de la Recherche Scientifique/Institut National de Physique Nucléaire et de Physique des Particules in France, the Agenzia Spaziale Italiana and the Istituto Nazionale di Fisica Nucleare in Italy, the Ministry of Education, Culture, Sports, Science and Technology (MEXT), High Energy Accelerator Research Organization (KEK), and Japan Aerospace Exploration Agency (JAXA) in Japan, the K. A. Wallenberg Foundation, the Swedish Research Council, and the Swedish National Space Board in Sweden. MASTER equipment was supported by Lomonosov MSU development program.

References

Abadie, J., Abbott, B. P., Abbott, R., et al. 2011, ApJ, 734, L35
Abbott, B., Abbott, R., Adhikari, R., et al. 2007, Phys. Rev. D, 76, 062003
Abbott, B. P., Abbott, R., Abbott, T. D., et al. 2019, ApJ, 874, 163
Abbott, B., Abbott, R., Abbott, T. D., et al. 2020, Liv. Rev. Rel., 23, 3
Abbott, R., Abbott, T. D., Acernese, F., et al. 2021, Phys. Rev. D, 104, 102001
Acernese, F., Agathos, M., Agatsuma, K., et al. 2014, CQG, 32, 024001
Ajello, M., Atwood, W. B., Axelsson, M., et al. 2021, Nat. Astron., 5, 385
Atwood, W. B., Abdo, A. A., Ackermann, M., et al. 2009, ApJ, 697, 1071
Bak, P., Christensen, K., Danon, L., & Scanlon, T. 2002, Phys. Rev. Lett., 88, 178501
Band, D., Matteson, J., Ford, L., et al. 1993, ApJ, 413, 281
Baring, M. G. 1993, ApJ, 418, 391
Barthelmy, S. D., Barbier, L. M., Cummings, J. R., et al. 2005, Space. Sci. Rev., 120, 143
Bellm, E. C., Kulkarni, S. R., Graham, M. J., et al. 2019, PASP, 131, 018002
Bhat, P. N., Meegan, C. A., Von Kienlin, A., et al. 2016, ApJS, 223, 28
Bloom, J. S., Frail, D. A., & Sari, R. 2001, AJ, 121, 2879
Bochenek, C. D., Ravi, V., Belov, K. V., et al. 2020, Nature, 587, 59
Burns, E., Veres, P., Connaughton, V., et al. 2018, ApJ, 863, L34
Burns, E., Svinkin, D., Hurley, K., et al. 2021, ApJ, 907, L28
Carilli, C. L., Holdaway, M. A., Ho, P. T. P., & de Pree, C. G. 1992, ApJ, 399, L59
Chand, V., Joshi, J. C., Gupta, R., et al. 2021, Res. Astron. Astrophys., 21, 236
Cheng, B., Epstein, R. I., Guyer, R. A., & Young, A. C. 1996, Nature, 382, 518
CHIME/FRB Collaboration (Amiri, M., et al.) 2021, ApJS, 257, 59
Connaughton, V., Briggs, M., Goldstein, A., et al. 2015, ApJS, 216, 32
Cummings, J. R. 2015, GRB Coordinates Network, 17267
Duncan, R. C., & Thompson, C. 1992, ApJ, 392, L9
Feroci, M., Frontera, F., Costa, E., et al. 1999, ApJ, 515, L9
Fong, W., Margutti, R., Chornock, R., et al. 2016, ApJ, 833, 151
Frederiks, D. D., Palshin, V. D., Aptekar, R. L., et al. 2007, Astron. Lett., 33, 19
Gaensler, B. M. 2004, Adv. Space Res., 33, 645
Goldstein, A., Veres, P., Burns, E., et al. 2017, ApJ, 848, L14
Goldstein, A., Cleveland, W. H., & Kocevski, D. 2022, Fermi GBM Data Tools: v1.1.1, `https://fermi.gsfc.nasa.gov/ssc/data/analysis/gbm`
Göğüş, E., Woods, P. M., Kouveliotou, C., et al. 1999, ApJ, 526, L93
Graham, M. J., Kulkarni, S. R., Bellm, E. C., et al. 2019, PASP, 131, 078001
Gruber, D., Goldstein, A., von Ahlefeld, V. W., et al. 2014, ApJS, 211, 12
Hurley, K. 2011, Adv. Space Res., 47, 1337
Hurley, K., Cline, T., Mazets, E., et al. 1999, Nature, 397, 41
Hurley, K., Boggs, S. E., Smith, D. M., et al. 2005, Nature, 434, 1098
Hurley, K., Rowlinson, A., Bellm, E., et al. 2010, MNRAS, 403, 342
Karachentsev, I. D., Makarov, D. I., & Kaisina, E. I. 2013, AJ, 145, 101
Kaspi, V. M., & Beloborodov, A. M. 2017, ARA&A, 55, 261
Kaspi, V. M., Gavriil, F. P., Woods, P. M., et al. 2003, ApJ, 588, L93
Kojima, Y. 2022, ApJ, 938, 91
Krolik, J. H., & Pier, E. A. 1991, ApJ, 373, 277
Lander, S. K. 2023, ApJ, 947, L16
Lander, S. K., Andersson, N., Antonopoulou, D., & Watts, A. L. 2015, MNRAS, 449, 2047
Leroy, A. K., Sandstrom, K. M., Lang, D., et al. 2019, ApJS, 244, 24
LIGO Scientific Collaboration (Aasi, J., et al.) 2015, CQG, 32, 074001
Lin, L., Kouveliotou, C., Göğüş, E., et al. 2011, ApJ, 740, L16
Lipunov, V., Kornilov, V., Gorbovskoy, E., et al. 2010, Adv. Astron., 2010, 1
Lipunov, V. M., Kornilov, V. G., Zhirkov, K., et al. 2022, Universe, 8, 271
Macquet, A., Bizouard, M.-A., Burns, E., et al. 2021, ApJ, 918, 80
Mazets, E., Golenetskii, S., Il'Inskii, V., Aptekar', R., & Guryan, Y. A. 1979, Nature, 282, 587
Mazets, E. P., Cline, T. L., Aptekar', R. L., et al. 1999, Astron. Lett., 25, 635
Mazets, E., Aptekar, R., Cline, T., et al. 2008, ApJ, 680, 545
Meegan, C., Lichti, G., Bhat, P., et al. 2009, ApJ, 702, 791
Mereghetti, S., Rigoselli, M., Salvaterra, R., et al. 2024, Nature, 629, 58
Minaev, P. Y., Pozanenko, A. S., Grebenev, S. A., et al. 2024, Astron. Lett., 50, 1
Nakar, E., & Piran, T. 2002, MNRAS, 330, 920
Negro, M., & Burns, E. 2023, in Neutron Star Astrophysics at the Crossroads: Magnetars and the Multimessenger Revolution, eds. E. Troja, & M. G. Baring, 363, 284
Norris, J. P., Hertz, P., Wood, K. S., & Kouveliotou, C. 1991, ApJ, 366, 240
Ofek, E. O. 2007, ApJ, 659, 339
Ofek, E. O., Kulkarni, S., Nakar, E., et al. 2006, ApJ, 652, 507
Ofek, E. O., Muno, M., Quimby, R., et al. 2008, ApJ, 681, 1464

Olausen, S. A., & Kaspi, V. M. 2014, ApJS, 212, 6
Paczynski, B. 1992, Acta Astron., 42, 145
Palmer, D. M., Barthelmy, S., Gehrels, N., et al. 2005, Nature, 434, 1107
Perley, R., Chandler, C., Butler, B., & Wrobel, J. 2011, ApJ, 739, L1
Petroff, E., Barr, E. D., Jameson, A., et al. 2016, PASA, 33, e045
Planck Collaboration VI. 2020, A&A, 641, A6
Roberts, O. J., Veres, P., Baring, M. G., et al. 2021, Nature, 589, 207
Scargle, J. D., Norris, J. P., Jackson, B., & Chiang, J. 2013, ApJ, 764, 167
Svinkin, D. S., Hurley, K., Aptekar, R. L., Golenetskii, S. V., & Frederiks, D. D. 2015, MNRAS, 447, 1028
Svinkin, D., Frederiks, D., Hurley, K., et al. 2021, Nature, 589, 211
Thompson, C., & Duncan, R. C. 1995, MNRAS, 275, 255
Thompson, C., & Duncan, R. C. 1996, ApJ, 473, 322
Troja, E., Ryan, G., Piro, L., et al. 2018, Nat. Commun., 9, 4089
Usov, V. V. 1984, Ap&SS, 107, 191
von Kienlin, A., Arend, N., Lichti, G. G., Strong, A. W., & Connell, P. 2003, in X-Ray and Gamma-Ray Telescopes and Instruments for Astronomy, eds. J. E. Truemper, & H. D. Tananbaum, SPIE Conf. Ser., 4851, 1336
Von Kienlin, A., Meegan, C. A., Paciesas, W. S., et al. 2014, ApJS, 211, 13
Von Kienlin, A., Meegan, C., Paciesas, W., et al. 2020, ApJ, 893, 46
Wang, Y., Wei, Y.-J., Zhou, H., et al. 2023, ApJ, submitted [arXiv:2312.02848]
Yin, Y.-H. I., Zhang, Z. J., Yang, J., et al. 2024, ApJ, 963, L10

Appendix A: Time-resolved spectral analysis

Table A.1. Fixed 8ms intervals.

Time (ms)	E_p (keV)	α	Energy Flux ($\mathcal{F}$) ($\times 10^{-6}$ ergs s^{-1} cm^{-2})	L_{iso} ($\times 10^{47}$ erg$\cdot$ s^{-1})	E_{iso} ($\times 10^{45}$ erg)
			GRB 180128A		
-16:-8	510 ± 80	1.0	25.0 ± 5.0	0.40 ± 0.08	0.32 ± 0.06
-8:0	510 ± 80	1.0	27.0 ± 5.0	0.4 ± 0.1	0.36 ± 0.07
0:8	300 ± 80	1.0	6.0 ± 2.0	0.10 ± 0.03	0.08 ± 0.03
8:16	260 ± 70	1.0	4.0 ± 2.0	0.07 ± 0.03	0.06 ± 0.02
16:24	200 ± 90	1.0	1.8 ± 0.9	0.03 ± 0.02	0.023 ± 0.012
24:32	60 ± 30	1.0	0.3 ± 0.2	0.005 ± 0.004	0.004 ± 0.003
			GRB 200415A*		
-8:0	1210 ± 90	-0.29 ± 0.06	142 ± 5	2.32 ± 0.09	1.86 ± 0.07
0:8	1410 ± 160	0.1 ± 0.1	88 ± 5	1.45 ± 0.08	1.15 ± 0.06
8:16	1100 ± 110	0.7 ± 0.2	75 ± 5	1.23 ± 0.08	0.98 ± 0.07
16:24	870 ± 90	1.1 ± 0.4	60 ± 4	0.99 ± 0.08	0.79 ± 0.6
24:32	950 ± 150	0.1 ± 0.2	38 ± 3	0.62 ± 0.05	0.50 ± 0.04
32:40	800 ± 110	0.7 ± 0.3	38 ± 3	0.62 ± 0.05	0.50 ± 0.04
40:48	860 ± 110	0.7 ± 0.3	40 ± 3	0.70 ± 0.06	0.53 ± 0.05
48:56	720 ± 110	1.1 ± 0.5	36 ± 3	0.60 ± 0.05	0.48 ± 0.04
56:64	860 ± 170	0.2 ± 0.3	28 ± 3	0.46 ± 0.04	0.37 ± 0.03
64:72	660 ± 120	0.5 ± 0.4	25 ± 3	0.41 ± 0.04	0.33 ± 0.03
72:80	710 ± 180	0.2 ± 0.4	15 ± 2	0.25 ± 0.03	0.20 ± 0.03
80:88	510 ± 100	0.3 ± 0.4	14 ± 2	0.23 ± 0.03	0.19 ± 0.03
88:96	400 ± 90	0.6 ± 0.6	10 ± 2	0.17 ± 0.03	0.14 ± 0.02
96:104	700 ± 300	-0.2 ± 0.4	0.5 ± 0.6	0.17 ± 0.03	0.14 ± 0.02
104:112	370 ± 60	2.1 ± 1.2	8 ± 2	0.13 ± 0.02	0.11 ± 0.02
112:120	340 ± 50	1.6 ± 0.8	8.7 ± 1.4	0.14 ± 0.02	0.11 ± 0.02
120:128	240 ± 30	2.1 ± 1.2	4.8 ± 0.9	0.080 ± 0.014	0.062 ± 0.011
128:136	100 ± 10	0.5 ± 1.1	3.4 ± 1.1	0.05 ± 0.02	0.043 ± 0.015
			GRB 150101B		
-16:-8	800 ± 200	0.0	13 ± 4	7000 ± 2000	5400 ± 1600
-8:0	129 ± 16	0.0	39.9 ± 0.5	2000 ± 300	1600 ± 200
0:8	40 ± 10	0.0	0.83 ± 0.18	420 ± 90	340 ± 70
8:16	20 ± 12	0.0	0.24± 0.11	130 ± 60	100 ± 50
16:24	6 ± 3	0.0	0.30 ± 0.13	200 ± 100	160 ± 80
24:32	30 ± 11	0.0	0.40 ± 0.13	210 ± 70	170 ± 60
32:40	19 ± 12	0.0	0.25 ± 0.11	130 ± 70	100 ± 50
40:48	43 ± 13	0.0	0.54 ± 0.16	270 ± 90	220 ± 70
48:56	24 ± 9	0.0	0.38 ± 0.12	200 ± 60	160 ± 50
56:64	9 ± 3	0.0	0.53 ± 0.14	320 ± 80	240 ± 70

Notes. The fluence is from fitting the spectrum with a Comptonized function over a combined (NaI and BGO detectors) spectral range of 8 keV to 40 MeV. * Values for GRB 200415A taken from Roberts et al. (2021)